Modeling Structure Effects on Aggregation Kinetics in Colloidal Dispersions

Peter Sandkühler, Jan Sefcik, Marco Lattuada, Hua Wu, and Massimo Morbidelli
Swiss Federal Institute of Technology Zurich, Laboratorium für Technische Chemie/LTC, ETH Hönggerberg/HCI, CH-8093 Zürich, Switzerland

The time evolution of the cluster-mass distribution (CMD) during colloidal aggregation can be modeled using population balance equations, given that the matrix of the aggregation rate constant (kernel) is known. Although numerous aggregation kernels have been proposed, their validity is still a major open problem, particularly when the role of the internal structure of the aggregates is referred to. A procedure is presented for the discrimination among possible kernel expressions including the structure effect. For aggregation processes in the submicron range, information about size and structure of aggregates can be obtained by dynamic and static light-scattering measurements, for example, in terms of the average hydrodynamic (R_h) and gyration (R_g) radii. These quantities can also be calculated from the cluster-mass distribution when accounting for the aggregate structure by the fractal concept and for the angular and rotational diffusion dependence of R_h. Since R_h and R_g represent different averages of the CMD, their simultaneous fitting is a severe test for a given kernel due to its inclusion of information on the average and width of the distribution. This procedure allows differentiation among several types of kernels proposed in the literature for DLCA and RLCA based on their ability to describe experimental data.

Introduction

Processing of colloidal suspensions, such as polymeric latexes, inorganic oxides, or complex biological systems, is an important step in the production of particulate materials for numerous technological applications. Such materials often need to be prepared in the form of powders or slurries in order to undergo further processing, such as extrusion, molding, casting, or coating. The application properties of the powders or slurries can be controlled through the aggregation processing step, wherein the primary particles, typically smaller than 100 nm, are arranged into aggregates with sizes ranging from a few microns up to a few millimeters. The structure, shape, and mechanical properties of the aggregates impact greatly the quality of the final powder and slurry, and are determined to a considerable extent by the processing conditions, which include the shear field, the solid volume fraction, and the amount of destabilizer added. Aggregates of solid primary particles are typically random, open structures, that can be characterized by a scaling relationship between their mass and size using the concept of fractal dimension (Forrest and Witten, 1979; Witten and Sander, 1981). It is important to monitor, predict, and control the mass and structure of the aggregates as they evolve in time during their processing. The final cluster-mass distribution (CMD) and particle-size distribution (PSD), which obviously depend crucially on the processing conditions, are in fact the key properties that determine the product quality.

To understand and to control the aggregate structure and the resulting CMD as desired for a specific application, it is necessary to develop quantitative models describing the aggregation under various processing conditions. The basic framework for such models are the population-balance (PB) equations (Ramkrishna, 2000). The important input into PB is the aggregation rate constant matrix (kernel), which depends on the operating conditions and various physicochemical characteristics of the aggregating dispersion. In general,

Correspondence concerning this article should be addressed to M. Morbidelli.

for stagnant systems of dispersed charged particles, the aggregation efficiency is determined by Van der Waals attractive and electrostatic repulsive interactions. The presence of shear can significantly enhance the aggregation rate through an increased aggregation frequency. In the case of spherical particles, it is possible to evaluate an aggregation rate constant or kernel that accounts for all such effects (c.f. Melis et al. (1999)). However, the situation becomes more complex when we consider random aggregates constituted of primary particles, and, therefore, characterized by a certain internal structure. Kernels for cluster aggregation under shear have been developed (Flesch et al., 1999; Kusters et al., 1997; Torres et al., 1991; Chung et al., 1998), but generally valid expressions have not been developed and rigorously tested yet. Although it is well recognized that the aggregation efficiency increases with aggregate mass, the detailed form of this dependence as well as the role of the internal aggregate structure remains an open question. Although in fact several types of kernels have been proposed in the literature, a systematic comparison of the corresponding CMD obtained by solving the PBE, with an appropriate experimental characterization of the CMD, is still missing. We intend to contribute to this analysis, focusing on quiescent colloidal systems both in the diffusion-limited (DLCA) and reaction-limited cluster aggregation (RLCA) regime.

The analysis of the structure and size of aggregates relies primarily on static and dynamic light-scattering techniques (Sorensen, 2000; Lin et al., 1990b,c), whose measurables are complex functions of the CMD. In principle, one could estimate the aggregation rate constants by starting from such measurements and solving the inverse problem in PB (Ramkrishna, 2000). However, the inverse problem approach requires quite reliable measurements of the entire CMD, which are quite unlikely to be accessible for aggregates in the submicron-size range.

Given this, the aim of this article is twofold: first we connect the framework of PB to the light-scattering theory in order to calculate the measurable quantities in the submicron-size range from the CMD obtained from PB. These quantities are the average hydrodynamic radius [R_h, measured by dynamic light-scattering (DLS)], and the average radius of gyration [R_g, measured by static light-scattering (SLS)], each one representing a different noninteger moment of the CMD. Second, we develop a procedure to distinguish between the functional forms of the aggregation kernels, based on the available experimental information about the CMD, namely, R_h and R_g in the submicron range. By solving the PB for the various kernels suggested in the literature, we demonstrate that using data on the evolution of both R_h and R_g compared to using just one of them, allows a significantly improved discrimination among different kernels, since by considering two different averages of the distribution we actually include information about the distribution width and shape. The discrimination procedure is illustrated for the DLCA and RLCA regimes in quiescent liquids, where unsuitable aggregation kernels can be excluded by comparing calculation results to experimental data on both R_h and R_g.

The article is organized as follows: in the following section we discuss the solution of PB and develop the connection between PB and light scattering. In the third section the aggregation rate constants (kernels) for the DLCA and RLCA regimes are introduced. Experimental results are shown in the fourth section, and we then present and discuss modeling results in the fifth section. We end with conclusions.

Aggregation Kinetics in Colloidal Systems

Population-balance equation

Population balances (PB) are general conservation laws applicable to a variety of particulate systems (Ramkrishna, 2000). Aggregation in homogeneously mixed colloidal dispersions can conveniently be described by PB, where we use mass as an internal coordinate for representing aggregates undergoing birth and death events. These events lead to the formation and disappearance of aggregates of mass m, and indicating with $f_1(m,t)$ the first-order product density function of aggregates of mass m at time t, we obtain the following form of the population balance

$$\frac{\partial f_1(m,t)}{\partial t} = \frac{1}{2}\int_0^m K(m-m',m')f_1(m-m',t)f_1(m',t)\,dm' - \int_0^\infty K(m,m')f_1(m,t)f_1(m',t)\,dm' \qquad (1)$$

where the two terms on the righthand side represent the rate of birth and death of units of mass m per unit volume, respectively. The first one represents the production of aggregates of mass m by aggregation of two smaller aggregates of mass $m-m'$ and m', while the second considers the loss of particles of mass m due to aggregation with any other aggregate of mass m'. The aggregation frequency function $K(m,m')$ accounts for two physical factors, which constitute the aggregation process: the collision frequency between two particles, and the corresponding sticking efficiency.

The validity of the PB in the form of Eq. 1 relies on several assumptions. In particular, in concentrated systems it can be expected that more than two particles undergo aggregation simultaneously and that the presence of the surrounding particles influences the two aggregating ones. On the other hand, in Eq. 1 only binary aggregation events are considered and the pair probability function $f_2(m,m',t)$, which accounts for the probability of finding two particles undergoing aggregation at the same spatial location in the time interval, Δt, is computed by assuming an independent probability of finding each of the two involved aggregates in the system, that is, $f_2(m,m',t) = f_1(m',t)f_1(m,t)$. This assumption is known as the closure hypothesis and has been discussed in the literature (Ramkrishna et al., 1976).

At the other extreme of diluted systems, where the population is constituted by only a few particles, it has been shown (Sampson and Ramkrishna, 1985) that the PB (Eq. 1) fails and single statistical events become important. This is due to the fact that in diluted systems the few particles present are correlated, meaning that the relation $f_2(m,m',t) = f_1(m',t)f_1(m,t)$ fails and higher-order product density functions $f_2(m,m',t)$, $f_3(m,m',m'',t)$, . . . , $f_M(m,m',m'',\ldots,m^M,t)$ have to be used in addition to the first-order functions used in Eq. 1.

No attempt is made in the following to *a priori* determine the upper and lower concentration bounds, where the aggre-

gation PB in the form of Eq. 1 is accurate. This would not be a straightforward task, and, therefore, we ultimately rely on the comparison with experimental data.

Numerical solution and reconstruction of the CMD

The description of aggregation phenomena in the framework of population balances requires the coverage of several orders of magnitude in aggregate size. Primary particles in colloidal dispersions usually are in the size range of 5–500 nm. Aggregation of these particles frequently results in clusters up to the size of 300 μm. Under certain operating conditions the formation of coagulum can occur, the radius of which can attain values up to 1–100 mm. Accordingly, in order to describe the evolution of the CMD over the whole range of particle and aggregate sizes, in particular cases up to 13 orders of magnitude using mass as an internal coordinate, have to be covered. Obviously, a simple linear discretization technique would result in a number of coupled ODEs not solvable in reasonable computer time. Thus, the application of a geometric or other expanding grids for the representation of particle sizes is indispensable for computational efficiency. In particular, the discretization method recently developed by Kumar and Ramkrishna (1996) (subsequently referred to as the *KR* method) has been adopted in this work.

According to the *KR* method, the entire size range of interest is discretized into intervals, and the particles and aggregates inside each interval are assigned to the boundaries (pivots) of the intervals themselves. This means that a cluster with mass m in the size range $\{m_k,m_{k+1}\}$ is split by two assigning fractions $g(m,m_k)$ and $h(m,m_{k+1})$ to the pivot populations at m_k and m_{k+1}, respectively. By properly selecting such assigning functions, it is possible to conserve two general properties, usually two moments, of the original distribution. The detailed description of the method is provided in the original article (Kumar and Ramkrishna, 1996). Vanni (2000) recently tested various discretization techniques, including the *KR* method, in terms of accuracy, ability to produce error estimates, ease of implementation, and computational speed, and concluded that the *KR* method is the most versatile and accurate one among those tested.

One important aspect that is often neglected is the reconstruction of the continuous distribution from the discretized one obtained from the numerical method (Butte et al., 2002). To illustrate this point we consider the PBE (Eq. 1) with a constant aggregation kernel, that is, $K(m,m')=K_B$, for which an analytical solution exists

$$N_i(t)=N_0(K_BN_0t)^{i-1}(1+K_BN_0t)^{-i-1} \qquad (2)$$

where N_i denotes the number of clusters of a certain dimensionless mass $i=m_i/m_1$, where m_i is the mass of a cluster with i primary particles and m_1 is the primary particle mass. In Figure 1a the discretized solution obtained with the *KR* method is compared with the corresponding values obtained using the analytical solution (Eq. 2). Note that these latter values are obtained by considering each one of the intervals $\Delta m=m_{k+1}-m_k$ defined by the *KR* method and summing up the numbers of aggregates having mass m_i lying between m_k and m_{k+1}. It is seen that the obtained values are in satisfactory agreement, thus indicating that the numerical *KR* method provides reliable results. The next point is to reconstruct from the discretized results in Figure 1a the complete solution, that is, the continuous solution given by Eq. 2. This is done by assuming an N_i constant in each discretization interval. The obtained results are compared in Figure 1b, and again the agreement is satisfactory, thus indicating that, although very simple, this reconstruction procedure provides reliable results, at least in the case under examination. It should be noted, however, that the distributions in Figures 1a and 1b are significantly different, as they in fact should be, since they represent different quantities. Care must therefore be taken in considering numerical solutions before and after reconstruction.

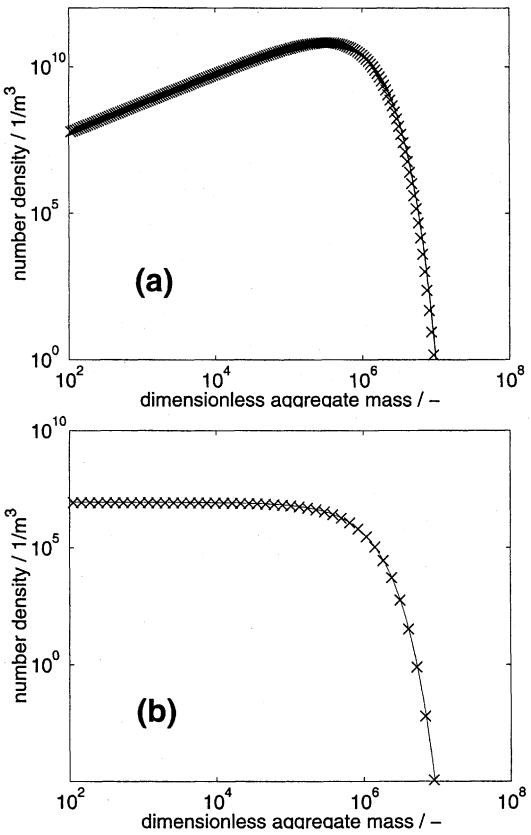

Figure 1. Comparison between the analytical (Eq. 2) and the numerical *KR* solution for Eq. 1 with the constant kernel $K(m,m')=K_B$.

(a) Discretized analytical solution (×), *KR* numerical solution (solid line); (b) continuous analytical solution (×), and reconstructed numerical *KR* solution (solid line). The geometric grid factor is $F=1.07$; the number of grid points is 300.

For the computations reported in this work we apply a geometric grid factor $F=m_{k+1}/m_k=1.07$ and a number of $M=300$ grid points, resulting in an upper bound of the grid equal to $m_M/m_1=6\times10^8$. The computation time for the preceding runs on an HP-3000 Unix workstation are 3 min for a simulated time of 1,000 min.

Another relevant point in computing CMDs numerically is that the size range for the problem on hand has to be specified *a priori* by an upper and a lower bound, here conve-

niently denoted in terms of aggregate mass m_1 and m_M, where M denotes the number of pivots in the discretized interval of aggregate mass. It should be noted that if the aggregates grow to such an extent that they reach the upper bound, and this is allowed to undergo further aggregation, the generated aggregates would be lost, since they would exit the discretized size range and consequently the mass of the dispersed phase would not be conserved. To avoid this, we have to close the boundary by a collective pivot (that is, the largest size m_M), which includes all aggregates larger than m_M and is excluded from the aggregation process. By properly applying this closure procedure, it is possible to satisfy the mass balance, which is particularly useful when dealing with systems that can produce aggregates of a very large size, as in the case of polymer or colloidal gelation (Butte et al., 2002; Krall and Weitz, 1998). However, in all computations shown in this work this situation does not occur and the last pivot always contains a negligible mass.

Relevant characteristics of aggregate populations

In many applications one is interested in the size of the aggregates, expressed in terms of volume or radius. Since the PBE just discussed provides a CMD, the question arises as to how the mass of an aggregate can be related to its size. In the case of coalescing particles this is straightforward, since the spherical shape is conserved upon aggregation. In the case of aggregates constituted of primary particles that rigidly adhere at their surface contacting points, we obtain randomly shaped aggregates that are usually described through the fractal scaling relation (Sorensen, 2000)

$$i = \frac{m_i}{m_1} = k_g \left(\frac{R_{g,i}}{a} \right)^{d_f} \tag{3}$$

where d_f is the fractal dimension, m_1 and a denote the mass and radius of a primary particle, while m_i and $R_{g,i}$ those of an aggregate. The prefactor k_g is a constant of the order of unity (Sorensen and Roberts, 1997). The radius of gyration $R_{g,i}$ in Eq. 3 is connected to the hydrodynamic radius, $R_{h,i}$, by a factor β, typically of the order of one, depending on the fractal dimension, d_f (Lin et al., 1990b,c; Wiltzius, 1987)

$$\beta = \frac{R_{h,i}}{R_{g,i}} \tag{4}$$

Having set the fractal dimension value, Eqs. 3 and 4 provide the average aggregate radii $R_{g,i}$ and $R_{h,i}$ as a function of the corresponding mass, m_i.

In selecting a quantity to define the size of an aggregate, it is convenient to adhere to quantities that can be measured experimentally. The accessible average size of the aggregate population is the radius of gyration ($\langle R_g^2 \rangle$), when using static light scattering (SLS), and the mean hydrodynamic radius ($\langle R_{h,\mathrm{eff}} \rangle$), when using dynamic light scattering (DLS). In order to compare these experimental values with the cluster-mass distribution, N_i, obtained from Eq. 1, we need to relate the averages $\langle R_g^2 \rangle$ and $\langle R_{h,\mathrm{eff}} \rangle$ of the entire CMD to the corresponding radii of the individual aggregates of mass i, given by $R_{g,i}$ and $R_{h,i}$. In the case of the radius of gyration, which relates to the mass distribution inside the aggregate, such a relation is simply given by (Pusey et al., 1987)

$$\langle R_g^2 \rangle = \frac{\sum_{i=1}^{M} i^2 N_i R_{g,i}^2}{\sum_{i=1}^{M} i^2 N_i} \tag{5}$$

In the case of the hydrodynamic radius, which actually reflects the mobility of the aggregate, the corresponding relation is more complex, since it has to account for the effect of the measurement angle, the wavelength of light, and the medium refractive index (Lin et al., 1990b,c; Pusey et al., 1987)

$$\langle R_{h,\mathrm{eff}} \rangle = \frac{\sum_{i=1}^{M} i^2 N_i S_i(q)}{\sum_{i=1}^{M} i^2 N_i S_i(q) R_{h,i,\mathrm{eff}}^{-1}} \tag{6}$$

where $S_i(q)$ represents the structure factor of the aggregates of mass i and $R_{h,i,\mathrm{eff}}$ denotes the effective hydrodynamic radius including the effect of rotational diffusion. Among the various possibilities for computing the structure factors (Sorensen and Wang, 1999) we have chosen the Fisher–Burford relation not only for its simplicity but also because it has been shown to be quite accurate for aggregates having fractal dimensions equal to about 2 (Sorensen, 2000). This is given by

$$S_i(q) = \left[1 + \frac{2}{3d_f} \left(qR_{g,i} \right)^2 \right]^{-d_f/2} \tag{7}$$

where q denotes the scattering wave vector, given by the relation

$$q = \frac{4\pi n}{\lambda} \sin\left(\frac{\theta}{2} \right) \tag{8}$$

where n is the refractive index of the liquid medium, λ is the wavelength of the used light, and θ is the scattering angle. The effective hydrodynamic radius of a single aggregate, including the influence of rotational diffusion, can be expressed as (Lindsay et al., 1988)

$$\frac{R_{h,i}}{R_{h,i,\mathrm{eff}}} = 1 + \frac{1}{2\beta^2} \left[1 + \frac{3\partial \ln S_i(q)}{\partial \left(qR_{g,i} \right)^2} \right] \tag{9}$$

Substituting the expressions of the aggregates' gyration and hydrodynamic radii, $R_{g,i}$ and $R_{h,i}$, given by Eqs. 3 and 4 into Eqs. 5 and 6, we obtain the following expressions

$$\langle R_g^2 \rangle = \frac{k_g^{-2/d_f} a^2 \sum_{i=1}^{M} N_i i^2 i^{2/d_f}}{\sum_{i=1}^{M} N_i i^2} \tag{10}$$

$$\langle R_{h,\mathrm{eff}} \rangle = \frac{\sum_{i=1}^{M} i^2 N_i S_i(q)}{\sum_{i=1}^{M} i^2 N_i \frac{S_i(q)}{R_{h,i}} \left\{ 1 + \frac{1}{2\beta^2} \left[1 - \left(1 + \frac{2(qR_{g,i})^2}{3d_f} \right)^{-1} \right] \right\}} \tag{11}$$

which allow us to compute the experimentally accessible radii, $\langle R_g^2 \rangle$ and $\langle R_{h,\mathrm{eff}} \rangle$, from the CMD, obtained by solving the PBE (Eq. 1). Note that Eqs. 10 and 11 apply once the fractal nature of the aggregates formed during aggregation is established, and, thus, they do not reproduce the initial stages of aggregation, when mainly dimers and trimers are present. It is worth noting that the gyration and hydrodynamic radii represent different noninteger moments of the CMD, and, therefore, provide information not only on the average value but also on the polydispersity of the CMD. Accordingly, comparing calculated with experimental values of both $\langle R_g^2 \rangle$ and $\langle R_{h,\mathrm{eff}} \rangle$ is a challenging test for the reliability of an aggregation kernel, and, therefore, provides the possibility of discriminating among different kernels with respect to various aggregation conditions.

In order to compute $\langle R_g^2 \rangle$ and $\langle R_{h,\mathrm{eff}} \rangle$ from the preceding equations we need to know the fractal dimension, d_f. In principle this quantity is also measurable (Lin et al., 1990b,c), although it is exposed to some uncertainty in the early stages of aggregation, and anyway it is difficult to measure in more concentrated systems (Lattuada et al., 2001; Lach-Hab et al., 1998). This point will be investigated later, where we examine the dependence of $\langle R_g^2 \rangle$ and $\langle R_{h,\mathrm{eff}} \rangle$ on the fractal dimension.

Forms of the Aggregation Kernel

In this section we discuss kernel equations for DLCA and RLCA that have been presented earlier in the literature. Note that the influence of gravitational forces on the initially stable colloidal dispersions becomes important when aggregates reach sizes of approximately 1 μm, depending on particle density. The direct application of settling kernels to the PBE is not feasible in the context of Eq. 1, since one should introduce an additional external coordinate in the vertical direction to account for the disappearance of settled aggregates (Perigault et al., 2000). Therefore, in the following we neglect the influence of gravitational settling and do not elaborate this issue any further. We should also point out that internal restructuring of clusters is not considered in this work. Internal restructuring of aggregates changing the fractal dimension of the clusters during aggregation can be caused mainly by two mechanisms. The first occurs during reversible aggregation, where the interaction forces between the particles are so weak (of the order of few k_BT) that thermal fluctuations can take the structure apart. This is not the case in the systems under consideration, where the aggregates are relatively strong, being that the interparticle attraction forces are sufficiently large. The second mechanism could occur in irreversible aggregation, when the aggregates are susceptible to restructering by shear forces. Since no shear forces are present here, we also can exclude this restructuring mechanism, in accordance with Lin et al. (1990a).

DLCA-kernel

In the diffusion-limited aggregation regime every collision between aggregates or primary particles is successful. The first and basic aggregation kernel for DLCA was derived by von Smoluchowski (1917), accounting for the diffusive mobility ($\mathfrak{D}_i + \mathfrak{D}_j$) and the collision cross section ($R_i + R_j$) of aggregates. The diffusion coefficient $\mathfrak{D}$ can be related to the radius of an equivalent sphere by the Stokes–Einstein relation ($\mathfrak{D}_1 = k_BT/6\pi\eta a$). Using these relations and neglecting the size dependence of the aggregation rate by assuming equal-sized particles, one obtains the *constant* aggregation kernel

$$K_B = \frac{8k_BT}{3\eta} \tag{12}$$

To incorporate aggregate structure using the fractal concept, the aggregate size is assumed to scale with its mass according to Eq. 3. An equivalent scaling is assumed for the diffusion coefficient (Jullien, 1992), given by $\mathfrak{D}_i/\mathfrak{D}_1 = (i)^{-1/d_f}$. From these relations, we obtain

$$K_{ij} = K_B B_{ij} \quad \text{with}$$
$$B_{ij} = \frac{1}{4}\left(i^{-1/d_f} + i^{-1/d_f}\right)\left(i^{1/d_f} + j^{1/d_f}\right) \tag{13}$$

where B_{ij} is the matrix representing the collision cross section and the mobility of the two colliding aggregates. This kernel has been found to properly describe experimental data in DLCA (Odriozola et al., 1999).

RLCA-kernel

In reaction-limited aggregation only a fraction of collisions is successful in forming a new aggregate, due to the incomplete screening of the repulsive forces between particles. Considering primary particles, the reduced sticking efficiency due to repulsive forces and hydrodynamic interactions can be expressed by the Fuchs stability ratio (Melis et al., 1999)

$$W = 2a\int_{2a}^{\infty} \frac{\exp(V/k_BT)}{G(r)r^2}\, dr \tag{14}$$

where $G(r)$ accounts for squeezing of the fluid between two approaching primary particles, r is the center to center distance, and V is the particle interaction potential. This expression of the stability ratio applies only for primary particles and not for aggregates, which are composed of many primary particles. It has, in fact, been verified experimentally, that the reactivity of aggregates increases with their mass (Lin et al., 1990c; Broide and Cohen, 1990), and, therefore, an additional factor P_{ij} has been introduced in Eq. 13, leading to the following general RLCA kernel

$$K_{ij} = K_B W^{-1} B_{ij} P_{ij} \tag{15}$$

Let us review in the following the various RLCA kernels reported in the literature and recast them in the form introduced earlier.

Using theoretical scaling arguments, Ball et al. (1987) concluded that the efficiency of aggregation is determined by the larger of the two aggregating clusters through a power $\boldsymbol{\lambda}$. This parameter accounts for the increased aggregation efficiency of larger clusters due to a larger number of contact possibilities on their surface, and it has been shown to be in the range $\boldsymbol{\lambda} \in [1, 1.1]$. The resulting kernel can be written in terms of P_{ij} in Eq. 15 as follows

$$P_{ij} = k^{\boldsymbol{\lambda}}$$
$$k = \max\{i,j\} \tag{16}$$

Note that in this special case, according to the original work (Ball et al., 1987), the matrix B_{ij} is not used, that is, it is replaced by the identity matrix in Eq. 15. For the rest of the following expressions of P_{ij}, Eq. 13 has been used for the matrix B_{ij} in Eq. 15.

Other authors (Family et al., 1985) used the product kernel, given by

$$P_{ij} = (ij)^{\boldsymbol{\lambda}} \tag{17}$$

to simulate the CMD by a Monte Carlo technique in the RLCA regime. They compared the obtained results with those given by the dynamic scaling theory, where the CMD obtained by Monte Carlo simulations is represented by a dynamic scaling form. Relating these results to the Smoluchowski equation and using Eq. 17, they found a nontrivial behavior. In a study using the stochastic simulation method (Thorn and Seesselberg, 1994) and comparing the results to dynamic scaling theory as well as to experimental data (Broide and Cohen, 1990), several values of $\boldsymbol{\lambda}$ have been tested. There it has been pointed out that the asymptotic expressions of the dynamic scaling theory might not provide the exponent $\boldsymbol{\lambda}$ sufficiently accurately. In RLCA experiments using silica (Axford, 1997), it has been found that the value of $\boldsymbol{\lambda}$ can vary in the range [0.36, 0.495], depending upon the solution ionic strength. These two studies suggest that, although the parameter $\boldsymbol{\lambda}$ determines how fast the reactivity of clusters grows with size, and, therefore, strongly affects the resulting CMD, its proper evaluation remains an open issue.

Schmitt et al. (2000) proposed relating the reactivity of a fractal aggregate in the DLCA regime to the number of primary particles located in its outer shell. Applying this idea to RLCA, we first compute the number of primary particles in the shell of an aggregate with a thickness equal to the diameter of a primary particle. The number of particles is calculated by substracting the number of particles in the core of the aggregate (without the shell) from the number of particles in the whole aggregate, using in both cases the fractal scaling relation $i = k_g(R_g/a)^{d_f}$ (Schmitt et al., 2000). We find that the number of primary particles in an aggregate of mass i is given by $P_i = i - (i^{1/d_f} - 1)^{d_f}$. Consequently, the aggregation efficiency of two aggregates i and j is given by

$$P_{ij} = P_i P_j = \left[i - \left(i^{1/d_f} - 1\right)^{d_f} \right] \left[j - \left(j^{1/d_f} - 1 \right)^{d_f} \right] \tag{18}$$

In order to investigate the scaling behavior of P_i, let us expand the equation in a Taylor series. First we rewrite P_i in the form $P_i = i\{1 - (1 - (1/i)^{1/d_f})^{d_f}\}$. Expanding the second factor in a Taylor series for $(1/i) \to 0$, we get that as $i \to \infty$, $P_i \to (i)^{(d_f - 1)/d_f}$, which is identical to the product kernel (Eq. 17) with an exponent $\boldsymbol{\lambda} \sim (d_f - 1)/d_f$ of the order of 0.5.

Another kernel previously used to model RLCA (Weitz and Lin, 1986; von Schulthess et al., 1980) is the sum kernel. Such a kernel can be derived by extending the concept of the stability ratio (Eq. 14), originally applied to the interaction potentials between primary particles, to the interaction potentials between aggregates. The stability ratio in Eq. 14 for strong repulsive interaction potentials in the RLCA limit can be approximated as $W = k \exp(V_{\max}/k_B T)$ (Reerink and Overbeek, 1954), where k is a function of primary particle size and $V_{\max}$ is the maximum potential at the distance $r_{\max}$ between centers of two approaching particles. Now let us also apply the stability ratio in Eq. 14 to aggregates with radii R_i and R_j and use the same $V_{\max}$ and $r_{\max}$ as for primary particles, since these are the contact points between aggregates. Furthermore, we assume a vanishing influence of $G(r,1)$ for larger aggregates and fold k into W. Then the stability ratio for two aggregates W_{ij} can be expressed as follows

$$W_{ij} = \left(R_i + R_j\right) \exp(V_{\max}/k_B T)/r_{\max}^2 = \frac{\left(R_i + R_j\right) \exp(V_{\max}/kT)}{\left(R_i + R_j + s_{\max}\right)^2} \tag{19}$$

where we substitute the maximum distance $r_{\max}$ by $(R_i + R_j + s_{\max})$, the sum of the radii of the clusters, and the distance $s_{\max}$ of the maximum interaction energy between two approaching aggregates. Since $s_{\max}$ is very small compared to the aggregate size R_i, we can simplify Eq. 19 ($R_i + R_j + s_{\max} \sim R_i + R_j$). Then by using Eq. 3 we can rewrite it in terms of Eq. 15 as $W_{ij} = W/P_{ij}$, where

$$P_{ij} = \frac{1}{2}\left(i^{1/d_f} + j^{1/d_f}\right) \tag{20}$$

so that the aggregation efficiency is proportional to the sum of the aggregate sizes.

It is worth noting that, since DLCA represents the upper limit of the cluster aggregation rate (Family et al., 1985), for all kernels we empirically correct the matrix P_{ij} by restricting its values to the range $P_{ij} \in [1; W]$. This corresponds to the experimentally observed transition from RLCA to DLCA, which occurs as the aggregate size increases in time (Lin et al., 1990c; Cametti et al., 1989).3

Odriozola et al. (2001) recently proposed an extension of the product kernel that accounts intrinsically for the RLCA to DLCA transition mentioned earlier. Rewritten in terms of Eq. 15, this kernel is given by

$$P_{ij} = \frac{\mathfrak{N}_{11}(ij)^{\boldsymbol{\lambda}}}{\left[1 + W^{-1}\left(\mathfrak{N}_{11}(ij)^{\boldsymbol{\lambda}} - 1\right)\right]} \tag{21}$$

It can be seen that as the aggregate masses increase from very low to very large values, the preceding expression predicts a smooth transition of the value of $W^{-1}P_{ij}$ from the RLCA limit $W^{-1}\mathfrak{N}_{11}(ij)^{\boldsymbol{\lambda}}$, that is, the product kernel, to the value of one predicted for the DLCA regime by Eq. 13. Note that $\mathfrak{N}_{11}$ has been estimated by Odriozola et al. to have the

value 6.1. When comparing the stability ratio used herein to the one used for different kernels, the apparent W^{-1} has to be corrected by the factor $\mathfrak{N}_{11}$.

Experimental Results

In this section we introduce our own experimental data as well as others taken from the literature on aggregation in the DLCA and RLCA regime. These data have been selected in order to provide evidence for the behavior of both gyration and hydrodynamic radii and to allow discrimination among different kernels.

First we briefly discuss the experimental measurement of $\langle R_g^2 \rangle$ and $\langle R_{h,\mathrm{eff}} \rangle$, which for brevity we refer in the following as R_g and R_h, respectively. In a static light-scattering experiment the time-averaged scattered intensity, I, is measured as a function of the scattering angle, and, therefore, of the scattering wave vector, q, in a typical angular range of 10° to 150°. The average structure factor $S(q)$ of all aggregates is defined as $S(q)P(q) = I(q)/I(0)$, where $P(q)$ is the form factor of primary particles (Kerker, 1969). From the reciprocal of the product $S(q)P(q)$ measured experimentally we can estimate directly the average R_g using the Zimm-plot (Higgins and Benoit, 1994): $1/[S(q)P(q)] = 1 + (1/3)q^2R_g^2$. The average hydrodynamic radius R_h is obtained from a dynamic light-scattering experiment at a particular scattering angle, in which the intensity-weighted time-averaged autocorrelation function is measured. From this function the dynamic structure factor is calculated using the Siegert relation (Lin et al., 1990b,c; Pusey and van Megen, 1989), which is then fitted to estimate the effective diffusion coefficient of the aggregates. From this last quantity the average effective hydrodynamic radius R_h is then computed using the Stokes–Einstein relation.

Figure 2a shows as a function of time the radii, R_g and R_h, of the aggregates formed from TiO_2 aerosols with a mean radius of 35 nm (Wang and Sorensen, 1999). In the original work a fractal dimension of $d_f = 1.75$ has been measured, suggesting a DLCA-type regime. As can be seen in Figure 2b, the ratio R_g/R_h remains substantially constant in time, suggesting an underlying CMD that does not change its shape during aggregation. In Figure 2c are shown R_h data for the silica system (Lin et al., 1990c), which exhibit the exponential growth typical of the RLCA regime. In this case, the primary particles had size $a = 3.5$ nm and concentration $\phi = 1 \times 10^{-5}$, corresponding to very dilute conditions.

The data shown in Figures 3a and 3b have been obtained in this work using latexes of MFA (Ausimont SpA, Italy), produced by emulsion copolymerization of tetrafluoroethylene and perfluoromethylvinylether. This polymer has a refractive index equal to 1.35, which is very close to that of water (1.33), thus leading to water dispersions of low turbidity, which can then be well characterized using light-scattering techniques even at relatively large particle volume frac-

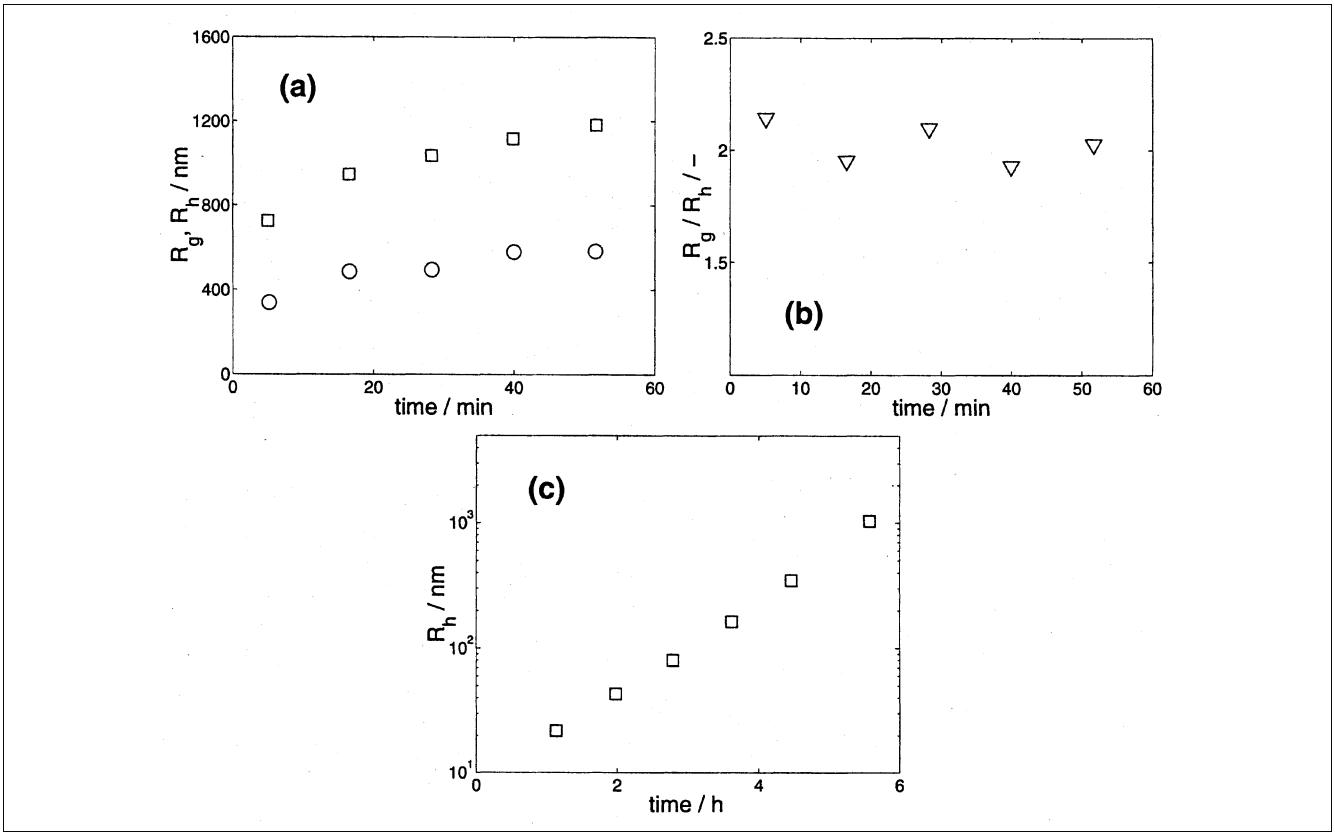

Figure 2. (a) Time evolution of R_g and R_h during DLCA for titania aerosol (Wang and Sorensen, 1999) [R_g(□), R_h (○)]; (b) ratio R_g/R_h (▽) for the same data as in (a); (c) time evolution of R_h during RLCA for silica aggregation in dispersion (Lin et al., 1990c).

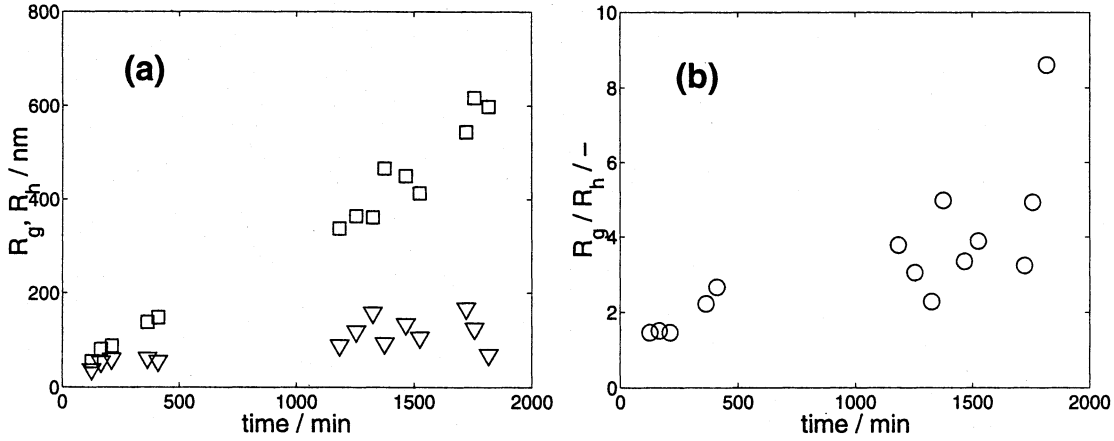

Figure 3. (a) and (b) Time evolution of aggregate size during DLCA for MFA latexes at $\phi = 0.02$ and $[Ca(NO_3)_2] = 0.002$ mol/L [R_g (□), R_h (△), R_g/R_h (○)].

tions. The primary particles used in the experiments have an average radius of 37.5 nm (polydispersity ~ 0.08), determined by DLS. The original latexes are diluted to the desired particle volume fraction using milli-Q (millipore) deionized water. The experiment has been performed using a final latex volume fraction of $\phi = 0.02$, and inducing aggregation by a final salt $[Ca(NO_3)_2]$ solution concentration of 0.002 mol/L. The time required to complete the experiments was about 33 h.

The aggregating samples were prepared starting from a latex obtained by diluting the original concentrated latex with deionized water in order to obtain a particle volume fraction of $\phi = 0.04$. Next, an appropriate aqueous solution of $[Ca(NO_3)_2]$ was prepared, so as to reach the desired final salt concentration after addition of the latex solution. The aggregating system was prepared by pouring the latex into the salt solution, without mechanical mixing, since shear stress affects the aggregation process. This procedure was designed in order to avoid local excess concentrations of either salt or latex. Each solution was prepared in large amounts (200 cc) in order to minimize experimental errors, and each aggregating sample was taken from the same solution and analyzed immediately after preparation. The light-scattering measurements (both static and dynamic) have been taken using a BI-200SM instrument (Brookhaven), using Argon laser (Lexel 95-2) light (wavelength $\lambda = 514.5$ nm), with angular range of the goniometer from 8° to 150°. Thanks to the low turbidity of the solution, SLS measurements were performed directly on the original aggregating solution. On the other hand, DLS measurements required proper dilution of the samples in order to avoid particle and aggregate interactions and to stop the aggregation process. As mentioned earlier, these are rather strong aggregates, so we do not expect any change in CMD or aggregate structure upon dilution.

Results and Discussion

DLCA

In the following we first present calculations performed for the DLCA process and compare them to the experimental data for gold, silica, and polystyrene colloids (Lin et al., 1990b). The time evolution of the hydrodynamic radius for an angle of 0° and the fractal dimension for each of the three systems have been measured experimentally. Consequently, the R_h calculations using the DLCA kernel (Eq. 13) are free of any fitting parameter. The results for the three different colloids are shown in Figure 4a. The agreement between the experimental data and the theoretical predictions for gold is very good. In the case of silica, an overprediction and in case of polystyrene, an underprediction is found. This discrepancy can be for several reasons. First, for silica, Lin et al. apply a solution with a pH above 11, where the silica particles are actually dissolving. The rate of this process is not known, but the thermodynamics (Sefcik and McCormick, 1997) clearly indicates that eventually silica will completely dissolve for the volume fraction used in these experiments. This observation suggests that it is reasonable to choose a smaller initial particle size, while keeping the initial number of particles constant, so as to take the silica dissolution into account. By directly fitting the experimental data a value for the initial radius of $a = 7.5$ nm, compared to the reported one of $a = 11$ nm, has been obtained (the corresponding calculated results are shown in Figure 4a by the lower and upper broken curves, respectively). Second, for polystyrene, the observed underprediction is surprising, since the aggregation rate calculated with the DLCA kernel has to be the fastest possible. This discrepancy may be due to small differences in the primary particle size or in the volume fraction, maybe in the sense of local concentration peaks due to mixing effects. In addition, we might have the effect of hydrodynamic interaction forces, which have been reported to change the aggregation rate in DLCA by a factor up to 2 (Spielman, 1970). However, it has to be noted that the slope of the R_h evolution in time is predicted correctly in all cases including the last one, thus confirming the reliability of the DLCA-kernel given by Eq. 13. It can be shown, in fact, that this slope is not affected by either the primary particle size or the volume fraction, ϕ.

The sensitivity of the results to the DLS measurement angle, indicated in the second section, is demonstrated in Figure 4b, where the experimental data taken at 42° (Lin et al., 1990b, Figure 6), along with the previous ones extrapolated to 0°, are compared with the model predictions. It is found that the slopes of the corresponding R_h time evolutions, ex-

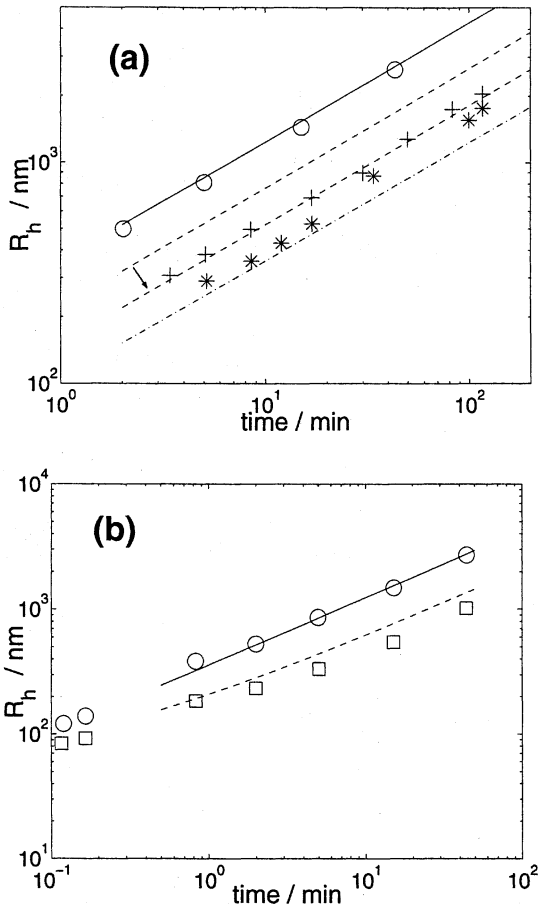

Figure 4. (a) Time evolution of R_h for DLCA for various colloids, symbols are experimental data (Lin et al., 1990b) and lines are calculations: gold (○,–), silica (+,– –) and polystyrene (∗,– ·), at angle 0° (arrows indicate adjustments of the model as discussed in the text); (b) effect of measurement angle on the R_h time evolution (Lin et al., 1990b) for experiments and calculations: 0° angle (○,–), 42° angle (□,– –).

perimental and calculated, are in good agreement and decrease as the measurement angle increases.

Figure 5 shows the ratio R_g/R_h as a function of time calculated using the DLCA kernel (Eq. 13), with $d_f = 1.8$ for various initial conditions in terms of volume fractions, ϕ, and initial radii, R_h, and for two measurement angles, that is, 0° and 90°, as indicated in the caption of the figure. It is seen that, as time increases, the ratio R_g/R_h, predicted for all volume fractions, and initial radii, converges to the same value, which depends only on the measurement angle. This shows that the evolution of the CMD in time in the DLCA regime exhibits scaling properties, meaning that basic parameters of the CMD, such as the R_g/R_h ratio, do not change in time, at least after a certain transient behavior. Such invariant characteristics of the CMD are attained earlier in time, the faster the DLCA process is, that is, the larger the initial number of primary particles is. Also the data shown in Figure 2b (Wang and Sorensen, 1999) exhibit a constant value for the ratio of R_g/R_h, again indicating scaling properties of the CMD. In

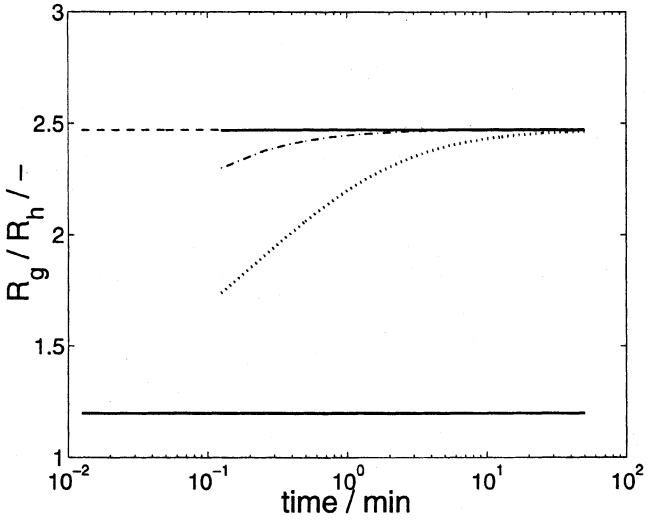

Figure 5. Time evolution of the ratio R_g/R_h for DLCA ($d_f = 1.8$) for various initial conditions and measurement angles calculated using the DLCA-kernel (Eq. 13).

For the angle of 90° the lines are: ((– –) $\phi = 0.01$, $a = 5$ nm, (– ·) $\phi = 1\times10^{-5}$, $a = 5$ nm, (—) $\phi = 0.01$, $a = 50$ nm, (· · ·) $\phi = 1\times10^{-5}$, $a = 50$ nm. The data at 0° for the identical conditions collapse to the lower solid curve (—).

this case, the experimental data were obtained at angles in the range between 20° and 50°. The value for the ratio R_g/R_h should therefore lie in between those computed for the angles 0° and 90° in Figure 5, as in fact it does.

RLCA

Let us first consider the experimental conditions in the RLCA regime adopted in getting the data for silica dispersions shown in Figure 2c (Lin et al., 1990c). In Figure 6a are shown the R_h time evolutions predicted by the different RLCA kernels, that is, kernel (Eq. 16) (Ball et al., 1987), the product kernel (Eq. 17), and its special case (Eq. 18), the sum kernels (Eq. 20) and (Eq. 21). In all cases, the same stability ratio, $W = 9.5\times10^5$, and the same values for the other involved parameter have been used, as summarized in Table 1, unless specifically noted. It is seen that the different kernels predict well-distinguishable R_h time evolutions, thus confirming the strong effect of the functional form of the P_{ij}-matrix. This means that one could easily discriminate among these different kernels, if an independent measurement of the stability ratio, W, was available. Although this is in principle possible, since W refers only to primary particles, such measurements are not available for the systems under consideration.

Therefore, in order to compare at least qualitatively the calculated data with the experimental values, in Figure 6b we modified the value of the stability ratio for each kernel as reported in Table 2 so as to obtain approximately the same experimental value $R_h = 100$ nm as in Figure 2c after 3 h. It appears that after this rescaling of the stability ratio, three kernels—those given by Eqs. 16, 17, and 21—are able to re-

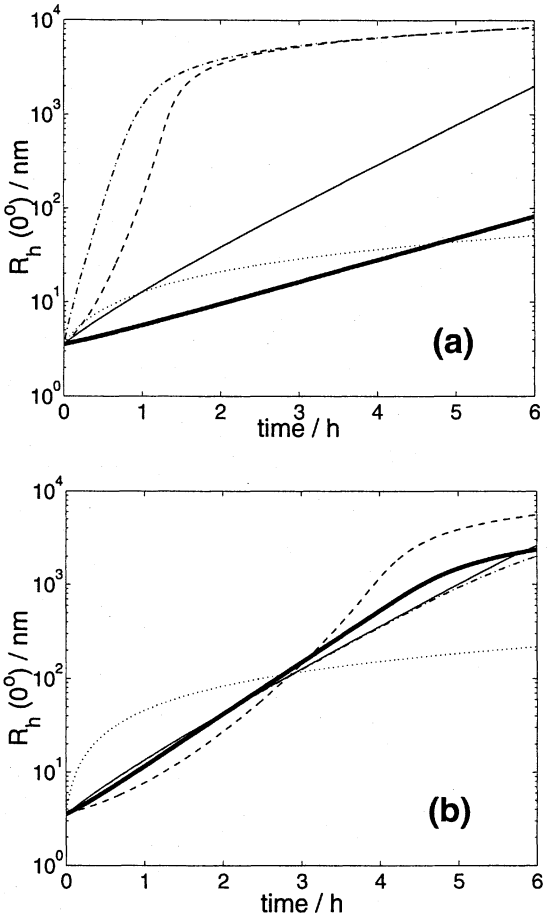

Figure 6. Time evolution of R_h at 0° predicted by various RLCA-kernels.

(a) Same $W = 9.5 \times 10^5$ for all kernels. (b) W values adjusted for each kernel to predict the experimental R_h after 3 h (see Figure 2c) as reported in Table 2. Lines: thick solid line Eq. 16, thin solid line Eq. 17, dashed-dotted Eq. 21, dashed Eq. 18, dotted Eq. 20.

Table 1. RLCA Kernel Parameters Used in All Calculations Unless Indicated Differently

Eq.	λ	d_f	$\mathfrak{N}_{11}$
16	1.0	2.12	–
17	0.5	2.12	–
18	–	2.12	–
21	0.5	2.12	6.1
20	–	2.12	–

produce the substantially linear growth of R_h in time exhibited by the experimental data in Figure 2c. Among these kernels a further distinction can be made by looking at the ratio R_g/R_h shown in Figures 7a and 7b for two different angles, 90° and 0°. The values of the ratio R_g/R_h predicted by Eqs. 16, 17, and 21 are initially very similar, but significant differences occur at later times. In particular, the time evolution of the ratio R_g/R_h for the kernel given by Eq. 16 is distinguishable from the remaining two, which are actually identical until the transition from RLCA to DLCA takes place. This is clearly due to the fact that the two kernels are identical, except that this transition is smoothened by the kernel given by Eq. 21. The conclusion is that three kernels, that is, Eqs. 16, 17, and 21, are capable of credibly reproducing the experimental trends in terms of R_h (Lin et al., 1990c). Most likely a distinction among these three kernels could be made if data also on the R_g time evolution were available.

Table 2. Stability Ratios Adjusted to Obtain Same R_h or R_g for All Kernels

Eq.	W in Figures 6b and 7	W in Figure 8
16	4.0×10^5	7.5×10^6
17	9.5×10^5	1.75×10^7
18	2.8×10^6	4.3×10^7
21	$5.5 \times 10^{6*}$	$1.1 \times 10^{8*}$
20	9.0×10^4	5.5×10^6

$^* = W\mathfrak{N}_{11}$.

The examination of the five RLCA kernels in the case of the MFA latexes aggregation is shown in Figure 8, where the time evolution of R_g and of the ratio R_g/R_h predicted by each of these kernels, is shown for the experimental system described in the context of Figures 3a and 3b. The stability ratio, W, has been adjusted for each kernel in order to ap-

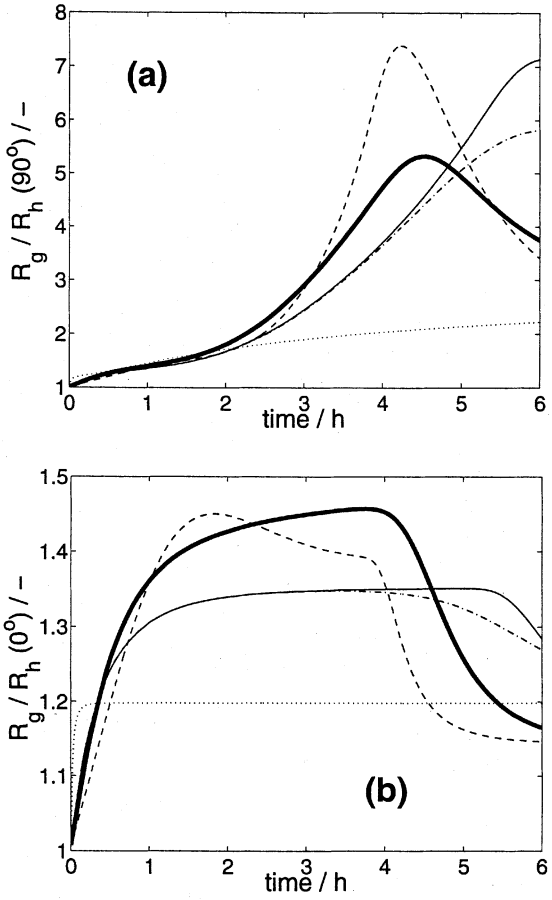

Figure 7. Time evolution of the ratio R_g / R_h for the same conditions as in Figure 6b.

(a) R_h at angle 90°. (b) R_h at angle 0°. Lines: thick solid line Eq. 16, thin solid line Eq. 17, dashed-dotted Eq. 21, dashed Eq. 18, dotted Eq. 20.

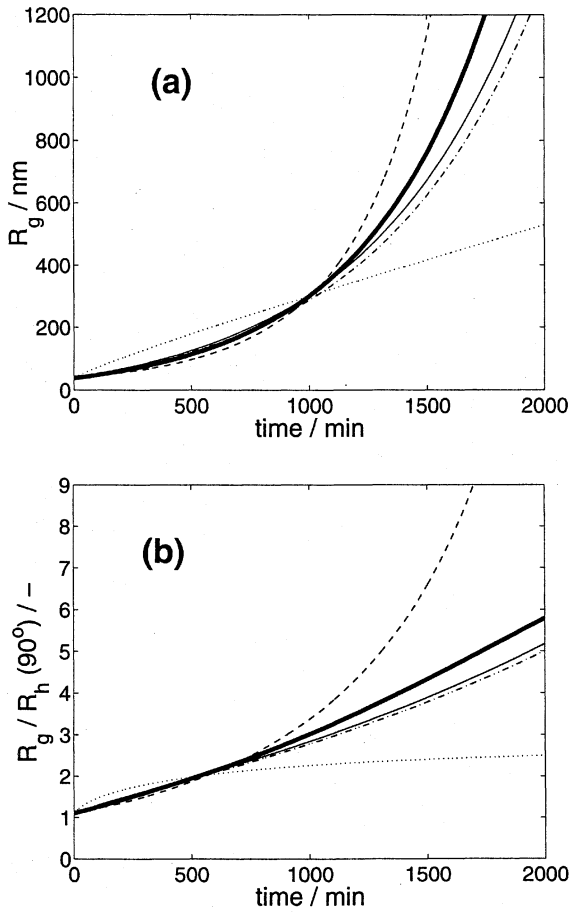

Figure 8. (a) Time evolution of R_g and (b) the ratio R_g/R_h for R_h at 90°, predicted by various RLCA kernels.

W values adjusted for each kernel to predict the experimental R_g at 1,000 min (see Figures 13a and 13b) as reported in Table 2. Lines: thick solid line Eq. 16, thin solid line Eq. 17, dashed-dotted Eq. 21, dashed Eq. 18, dotted Eq. 20.

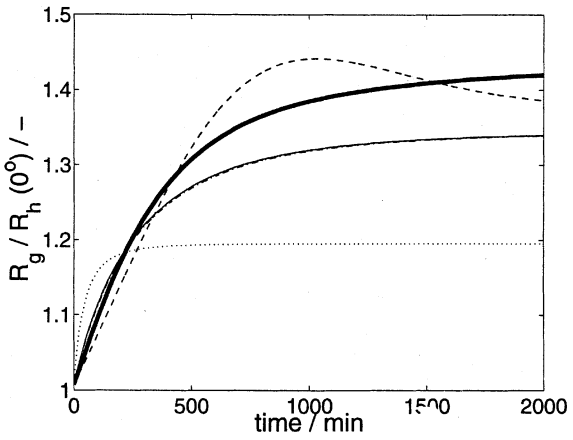

Figure 9. Time evolution of the ratio R_g/R_h with R_h at 0°.

Same conditions as in Figure 8. Lines: thick solid line Eq. 16, thin solid line Eq. 17, dashed-dotted Eq. 21, dashed Eq. 18, dotted Eq. 20.

proximately reproduce the R_g values observed experimentally in Figures 3a and 3b after 1,000 min ($R_g = 300$ nm). The obtained values of W are reported in Table 2.

In Figure 8 it is seen that four kernels—Eqs. 16, 17, 21, and 18—exhibit a similar R_g evolution in time. The additional examination of the ratio R_g/R_h reveals a distinctly different behavior of the kernel given by Eq. 18. However, it also appears that none of these kernels seems capable of reproducing the behavior of the experimental data exactly.

Figure 9 shows, for the same conditions considered in Figure 8, the values of the ratio R_g/R_h, with R_h computed at 0°, as a function of time. It is seen that the obtained time evolution is distinctly different from the one at 90° shown in Figure 8b. The results for an angle of 0° can be compared qualitatively to experimental data reported on silica aggregation in the RLCA regime (Wiltzius, 1987; Pusey et al., 1987), where the R_h and R_g time evolution extrapolated to an angle of 0° were measured and a value of $R_g/R_h = 1.39$ was obtained. When considering that the experimental system is different, we can conclude that this value is in reasonable agreement with the calculations shown in Figure 9 for at least four kernels.

The conclusion of this analysis is that in order to discriminate among the different RLCA kernels it would be convenient to use experimental values of not only one average size, but of two or more of them, such as R_h and R_g. Here it is worth pointing out that data on R_h at different scattering angles also contribute to better discrimination among the kernels, since they actually correspond to different averages of the CMD. Based on the currently available experimental data, the best qualitative reproduction of the data is given by the kernels given by Eqs. 16, 17, and 21, although a satisfactory agreement could not be achieved for all the systems considered. For the latter two, a significant improvement can be expected by operating on the additional adjustable parameter, λ, as discussed in the next section.

Influence of λ and d_f on the ratio R_g/R_h

In this section only the kernel given by Eq. 21 has been considered, since the one given by Eq. 17 gives substantially the same results, except for small deviations in the neighborhood of the transition from RLCA to DLCA. The effect of the parameter λ on the qualitative behavior of the values of R_g and of the ratio R_g/R_h as a function of time is demonstrated in Figures 10a and 10b. As pointed out in the third section when introducing the kernels, there is no general agreement about the value λ should take. Actually, there is no well-developed physical model behind the product kernel that can provide a solid foundation for its evaluation, and, therefore, we have to regard it at the moment as an adjustable parameter. In this context we note that the results shown in Figures 10a and 10b indicate that λ can have profound effects on the evolution of the CMD. In particular, in Figure 10a, following the arrow and considering the structure of the kernel given by Eq. 21, we see that at short times R_g increases as W decreases, thus overtaking the effect of λ that decreases; on the other hand, at later times, R_g decreases as λ decreases, although W increases. This demonstrates that

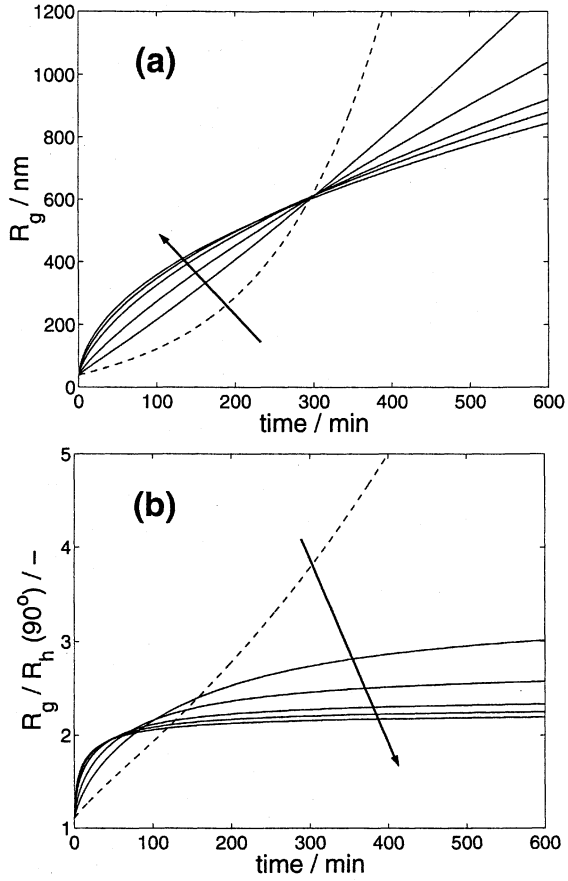

Figure 10. Influence of W and λ on the time evolution of (a) R_g and (b) R_g/R_h, according to kernel (Eq. 21) with all other parameters fixed.

Parameter combinations in direction of arrows: $W = 5.5 \times 10^6$ and $\lambda = 0.5$; $W = 1.6 \times 10^6$ and $\lambda = 0.3$; $W = 7.5 \times 10^5$ and $\lambda = 0.2$; $W = 3.25 \times 10^5$ and $\lambda = 0.1$; $W = 2.1 \times 10^5$ and $\lambda = 0.05$; $W = 1.5 \times 10^5$ and $\lambda = 0.01$.

W governs the initial aggregation rate, where the interactions between primary particles dominate. The exponent λ, however, governs the later stages of aggregation, when larger clusters are present and describes how the reactivity of the aggregates changes with the aggregate size.

Another parameter that has to be taken into consideration when trying to obtain kinetic information from the time evolution of R_g and R_h is the fractal dimension appearing in Eqs. 10 and 11. In order to illustrate the effect of this parameter, Figure 11 shows the calculated values of the ratio R_g/R_h as a function of time using the kernel given by Eq. 21 for various values of the fractal dimension, ranging from $d_f = 2.0$ to 2.2. This range is representative of the RLCA regime, with the lower limit crossing over to DLCA. Note that the effect of the fractal dimension is both on the expression of the kernel given by Eq. 21 as well as on the evaluation of R_g and R_h from the CMD through Eqs. 10 and 11. In principle, this parameter should, and to a certain extent can, be estimated experimentally independently of the CMD. This would allow the number of adjustable parameters to decrease and, therefore, to attain a more physically sound interpretation of the CMD data. However, the estimation of the fractal dimension

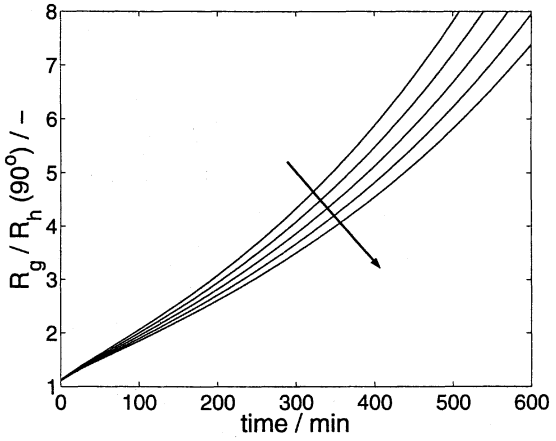

Figure 11. Influence of d_f on the R_g/R_h time evolution according to kernel (Eq. 21) with all other parameters fixed.

$W = 5.5 \times 10^6$, $\lambda = 0.5$. The changes in fractal dimension in the direction of arrow: $d_f = 2.0$; $d_f = 2.05$; $d_f = 2.1$; $d_f = 2.15$; $d_f = 2.2$.

from aggregates and gels is still an area of active research (Lattuada et al., 2001; Lach-Hab et al., 1998).

Conclusions

In this work we assess the validity of modeling the aggregation kinetics of colloidal systems in quiescent liquids using population-balance equations and appropriate kernels. For this, several typical sets of experimental data, developed by us and taken from the literature, have been considered. Since the early stages of the aggregation process in colloid systems occur in the submicron range, the measurement technique of choice is light scattering. From light-scattering measurements, two quantities are obtained as measures of aggregate size, namely, the radius of gyration and the hydrodynamic radius, where the latter further depends on the adopted scattering angle. Each of these quantities provides independent information on the CMD, and, therefore, combining them provides a significant test for the reliability of the simulation models. In order to perform such tests, we report appropriate equations for calculating the hydrodynamic radius and the radius of gyration from a given CMD.

Although the available experimental information is somehow limited, it is confirmed once again that in the DLCA regime the kernel given by Eq. 13 is sufficiently reliable, while for the RLCA regime the problem remains open. However, we conclude that only the product kernels (Eqs. 17 or 21), and within the limitation of having no free parameter, the kernel given by Eq. 16, are capable of reproducing at least qualitatively the observed experimental data, provided that some tuning is accepted on the exponent λ, and possibly on the fractal dimension, d_f.

It was demonstrated that a more definite conclusion about the reliability of this kernel can be achieved if more specific experimental measurements are available. These include, on one side, more detailed information on the shape of the CMD, which could be obtained through measurements of the ratio R_g/R_h, using various scattering angles for R_h. On the other

side, one could measure independently the stability ratio, W, which in the context of these kernels relates only to primary particles and, although experimentally more demanding, the fractal dimension of the aggregates, d_f.

In summary, a procedure was developed that allows more rigorous discrimination among aggregation kernels, providing valuable information about kernel expressions appropriate for various processing conditions. The concept has been demonstrated on stagnant systems, although it can easily be applied to aggregation under shear or turbulence.

Acknowledgments

This work was performed with financial support by the Swiss National Science Foundation (NSF), under Grant No. 2000-061883.

Notation

a = primary particle radius
B_{ij} = matrix of mobility and collision radii
d_f = fractal scaling exponent (fractal dimension)
$\mathfrak{D}$ = diffusion coefficient
F = geometric grid factor
$f_1(m,t)$ = first-order density function
$f_2(m,m',t)$ = second-order density function
$G(r)$ = hydrodynamic interaction function between particles
g,h = assigning fractions in *KR* method
$i,j,k = m_i/m_1$, dimensionless aggregate mass and index
K,K_{ij} = full matrix of aggregation kernel
k_g,k_h = prefactors in the fractal scaling relation Eq. 3
K_B = thermal energy of aggregation (Eq. 12)
k_B = Boltzmann constant
M = number of discretized grid points
m_i = mass of aggregate counting i primary particles
N_i = number of aggregates of mass i
N_0 = initial number of primary particles
$\mathfrak{N}_{11}$ = number of collisions per encounter [kernel (Eq. 21)]
n = refractive index
P_{ij} = matrix for aggregate reactivity
$P(q)$ = primary particle form factor
q = scattering wave vector
R_h = hydrodynamic radius
R_g = radius of gyration
r = center–center distance between particles
$S(q),S_i(q)$ = structure factor of population of aggregates or individual aggregate
s = interaggregate distance in kernel (Eq. 20)
t = time
T = temperature
V = particle interaction potential
W = stability ratio of primary particles
W_{ij} = concept of stability ratio of clusters

Greek letters

β = ratio between hydrodynamic radius and radius of gyration
Δ = interval width
η = dynamic viscosity
θ = scattering angle
$\boldsymbol{\lambda}$ = reactivity exponent in aggregation kernel
λ = wavelength of light
ϕ = initial volume fraction of particles

Literature Cited

Axford, S., "Aggregation of Colloidal Silica: Reaction-Limited Kernel, Stability Ratio and Distribution Moments," *J. Chem. Soc., Faraday Trans.*, **93**, 3030 (1997).

Ball, R., D. Weitz, T. Witten, and F. Leyvraz, "Universal Kinetics in Reaction-Limited Aggregation," *Phys. Rev. Lett.*, **58**, 274 (1987).

Broide, M., and R. Cohen, "Experimental Evidence of Dynamic Scaling in Colloidal Aggregation," *Phys. Rev. Lett.*, **64**, 2026 (1990).

Butte, A., G. Storti, and M. Morbidelli, "Evaluation of the Chain Length Distribution in Free-Radical Polymerization—1," *Macromol. Theory Simul.*, **11**, 22 (2002).

Cametti, C., P. Codastefano, and P. Tartaglia, "Aggregation Kinetics in Model Colloidal Systems: A Light Scattering Study," *J. Colloid Interface Sci.*, **131**, 409 (1989).

Chung, C.-B., S.-H. Park, I.-S. Han, Y.-H. Seo, and B.-T. Yang, "Modeling of ABS Latex Coagulation Processes," *AIChE J.*, **44**, 1256 (1998).

Family, F., P. Meakin, and T. Vicsek, "Cluster Size Distribution in Chemically Controlled Cluster-Cluster Aggregation," *J. Chem. Phys.*, **83**, 4144 (1985).

Flesch, J., P. Spicer, and S. Pratsinis, "Laminar and Turbulent Shear-Induced Flocculation of Fractal Aggregates," *AIChE J.*, **45**, 1114 (1999).

Forrest, S., and T. Witten, "Long-Range Correlations in Smoke-Particle Aggregates," *J. Phys. A — Math. Gen.*, **12**, L109 (1979).

Higgins, J., and H. Benoit, *Polymers and Neutron Scattering*, Oxford Science Publications, Clarendon Press, Oxford (1994).

Jullien, R., "The Application of Fractals to Colloidal Aggregation," *Croat. Chem. Acta*, **65**, 215 (1992).

Kerker, M., *The Scattering of Light*, Academic Press, New York (1969).

Krall, A., and D. Weitz, "Internal Dynamics and Elasticity of Fractal Colloidal Gels," *Phys. Rev. Lett.*, **80**, 778 (1998).

Kumar, S., and D. Ramkrishna, "On the Solution of Population Balance Equations by Discretization—I. A Fixed Pivot Technique," *Chem. Eng. Sci.*, **51**, 1311 (1996).

Kusters, K., J. Wijers, and D. Thoenes, "Aggregation Kinetics of Small Particles in Agitated Vessels," *Chem. Eng. Sci.*, **52**, 107 (1997).

Lach-Hab, M., A. Gonzalez, and E. Blaisten-Barojas, "Structure Function and Fractal Dimension of Diffusion-Limited Colloidal Aggregates," *Phys. Rev. E*, **57**, 4520 (1998).

Lattuada, M., H. Wu, and M. Morbidelli, "Estimation of Fractal Dimension of Colloidal Gels in the Presence of Multiple Scattering," *Phys. Rev. E*, **64**, 061404 (2001).

Lin, M. Y., R. Klein, H. M. Lindsay, D. A. Weitz, R. C. Ball, and P. Meakin, "The Structure of Fractal Colloidal Aggregates of Finite Extend," *J. Colloid Interface Sci.*, **137**, 263 (1990a).

Lin, M., H. M. Lindsay, D. A. Weitz, R. C. Ball, R. Klein, and P. Meakin, "Universal Diffusion-Limited Aggregation," *J. Phys.: Condens. Matter*, **2**, 3093 (1990b).

Lin, M., H. M. Lindsay, D. A. Weitz, R. Klein, R. C. Ball, and P. Meakin, "Universal Reaction-Limited Aggregation," *Phys. Rev. A*, **41**, 2005 (1990c).

Lindsay, H., M. Y. Lin, D. A. Weitz, R. C. Ball, R. Klein, and P. Meakin, "Light Scattering from Fractal Colloid Aggregates," *Proc. Photon Correlation Techniques and Applications Conf.*, Vol. 1, Washington, DC, p. 122 (1988).

Melis, S., M. Verduyn, G. Storti, M. Morbidelli, and J. Baldyga, "Effect of Fluid Motion on the Aggregation of Small Particles Subject to Interaction Forces," *AIChE J.*, **45**, 1383 (1999).

Odriozola, G., A. Moncho-Jorda, A. Schmitt, J. Callejas-Fernandez, R. Martinez-Garcia, and R. Hidalgo-Alvarez, "A Probabilistic Aggregation Kernel for the Computer-Simulated Transition from DLCA to RLCA," *Europhys. Lett.*, **53**, 797 (2001).

Odriozola, G., A. Schmitt, J. Callejas-Fernandez, R. Martinez-Garcia, and R. Hidalgo-Alvarez, "Dynamic Scaling Concepts Applied to Numerical Solutions of Smoluchowski's Rate Equation," *J. Chem. Phys.*, **111**, 7657 (1999).

Perigault, J., J. Leckie, and P. Kitanidis, "Modeling Particle Transport and Aggregation in a Quiescent Aqueous Environment Using the Residence-Time Scheme," *Water Resour. Res.*, **36**, 2249 (2000).

Pusey, P., J. Rarity, R. Klein, and D. Weitz, "Comment on 'Hydrodynamic Behavior of Fractal Aggregates'," *Phys. Rev. Lett.*, **59**, 2122 (1987).

Pusey, P., and W. van Megen, "Dynamic Light Scattering by Non-Ergodic Media," *Physica A*, **157**, 705 (1989).

Ramkrishna, D., *Population Balances*, Academic Press, San Diego, CA (2000).

Ramkrishna, D., B. Shah, and J. Borwanker, "Analysis of Population Balance—III," *Chem. Eng. Sci.*, **31**, 435 (1976).

Reerink, H., and J. Overbeek, "The Rate of Coagulation as a Measure of the Stability of Silver Iodide Sols," *Discuss. Faraday Soc.*, **18**, 74 (1954).

Sampson, K., and D. Ramkrishna, "Particle Size Correlations and the Effects of Limited Mixing on Agglomerating Particulate Systems," *J. Colloid Interface Sci.*, **104**, 269 (1985).
Schmitt, A., G. Odriozola, A. Moncho-Jorda, J. Callejas-Fernandez, R. Martinez-Garcia, and R. Hidalgo-Alvarez, "Multiple Contact Kernel for Diffusionlike Aggregation," *Phys. Rev. E*, **62**, 8335 (2000).
Sefcik, J., and A. McCormick, "Thermochemistry of Aqueous Silicate Solution Precursors to Ceramics," *AIChE J.*, **43**, 2773 (1997).
Sorensen, C., "Light Scattering by Fractal Aggregates: A Review," *Aerosol Sci. Technology*, **35**, 648 (2000).
Sorensen, C., and G. Roberts, "The Prefactor of Fractal Aggregates," *J. Colloid Interface Sci.*, **186**, 447 (1997).
Sorensen, C., and G. Wang, "Size Distribution Effect on the Power Law Regime of the Structure Factor of Fractal Aggregates," *Phys. Rev. E*, **60**, 7143 (1999).
Spielman, L., "Viscous Interactions in Brownian Coagulation," *J. Colloid Interface Sci.*, **33**, 562 (1970).
Thorn, M., and M. Seesselberg, "Dynamic Scaling in Colloidal Aggregation: Comparison of Experimental Data with Results of Stochastic Simulations," *Phys. Rev. Lett.*, **72**, 3622 (1994).
Torres, F., W. Russel, and W. Schowalter, "Floc Structure and Growth Kinetics for Rapid Shear Coagulation of Polystyrene Colloids," *J. Colloid Interface Sci.*, **142**, 554 (1991).
Vanni, M., "Approximate Population Balance Equations for Aggregation-Breakage Processes," *J. Colloid Interface Sci.*, **221**, 143 (2000).
Von Schulthess, G., G. Benedek, and R. DeBlois, "Measurement of the Cluster Size Distributions for High Functionality Antigens Cross-Linked by Antibody," *Macromolecules*, **13**, 939 (1980).
Von Smoluchowski, M., "Versuch einer mathematischen Theorie der Koagulationskinetic kolloider Lösungen," *Z. Phys. Chem.*, **92**, 129 (1917).
Wang, G., and C. Sorensen, "Diffusive Mobility of Fractal Aggregates Over the Entire Knudsen Number Range," *Phys. Rev. E*, **60**, 3036 (1999).
Weitz, D., and M. Lin, "Dynamic Scaling of Cluster-Mass Distributions in Kinetic Colloid Aggregation," *Phys. Rev. Lett.*, **57**, 2037 (1986).
Wiltzius, P., "Hydrodynamic Behavior of Fractal Aggregates," *Phys. Rev. Lett.*, **58**, 710 (1987).
Witten, T., and L. Sander, "Diffusion-Limited Aggregation, a Kinetic Critical Phenomenon," *Phys. Rev. Lett.*, **47**, 1400 (1981).

Manuscript received June 19, 2002, and revision received Nov. 27, 2002.